Electronic Supplementary Information (ESI):

Efficient Electron-promoted Desorption of Benzene from Water Ice Surfaces†

Demian Marchione*[a], John D. Thrower[b], and Martin R. S. McCoustra[a]

1 RAIR spectra of C_6H_6 on c-ASW

Temperature programmed desorption (TPD) data, reported in a previous work,[1] suggest that benzene (C_6H_6) is π-hydrogen bonded to the water (H_2O) ice interface in the sub-monolayer regime. Reflection-absorption infrared (RAIR) spectra for similar coverages support this interpretation with some evidence of small shifts in peak position of the aromatic C-C stretch from that of bulk C_6H_6.[2] **Figure 1** shows the evolution of the aromatic ring normal mode as the exposure of C_6H_6 on the icy film is increased from the sub-monolayer regime (1 L) to the bulk (20 L). This vibrational frequency appears to be sensitive enough to probe the change in the intermolecular interaction when

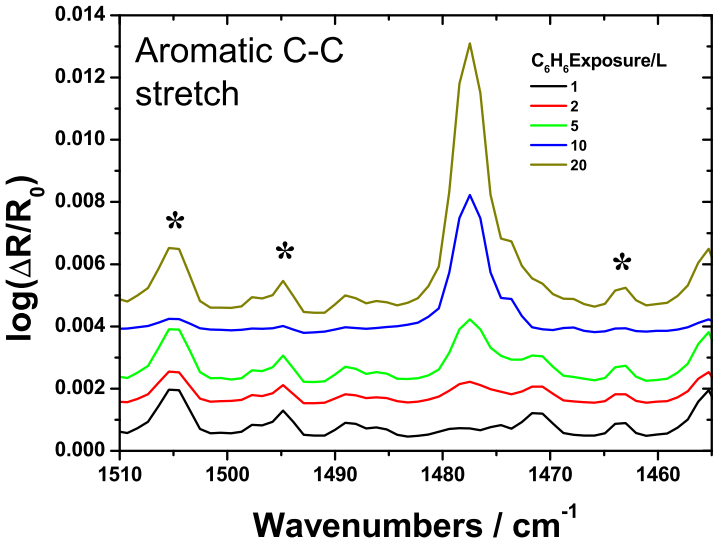

Figure 1 *RAIR spectra for 1-20 L of C_6H_6 deposited on a thick H_2O film an amorphous SiO_2 substrate. H_2O bands have been removed as part of the baseline correction. The features indicated by * are attributed to gas phase H_2O vapour in the beam path outside the UHV chamber.*

*[a] *Institute of Chemical Sciences, Heriot-Watt University, EH14 4AS, Edinburgh, UK; E-mail: dm290@hw.ac.uk*
[b] *Westfälische Wilhelms-Universität Münster, Münster, Germany; E-mail: john.thrower@uni-muenster.de*
[a] *Institute of Chemical Sciences, Heriot-Watt University, EH14 4AS, Edinburgh, UK; E-mail: mrsm1@hw.ac.uk*

switching between the two regimes. Thus, the observed shift from 1474 cm^{-1} to 1477 cm^{-1} is consistent with donation of π-electron density to a electrophilic centre (dangling OH).

2 CASINO Calculations

Monte Carlo simulations were performed to determine the electron penetration depth in pure C_6H_6 and compact amorphous solid water (c-ASW) films using version 2.48 of the CASINO code.[3,4] The incident beam was set at 60°, over an area of 1 mm^2, consistently with the experimental conditions (*e.g.* electron energy), while the average thickness of the films was estimated for each exposure as described in the article corresponding to this ESI (**Equation 1**). The ionisation coefficient[5] and molecular density[6] of C_6H_6 are 6.0 and 8.57×10^{21} molecule cm^{-3} respectively. For c-ASW the analogous values[7,8] of 1.1 and 2.91×10^{22} molecule cm^{-3} were employed for the simulations.

Figure 2 displays the penetration depth of 250 eV electrons in a pure thick C_6H_6 film (200 L, $\sim$ 7 nm), reported in black. The arrow and the red curve highlight the thickness estimated for 50 L

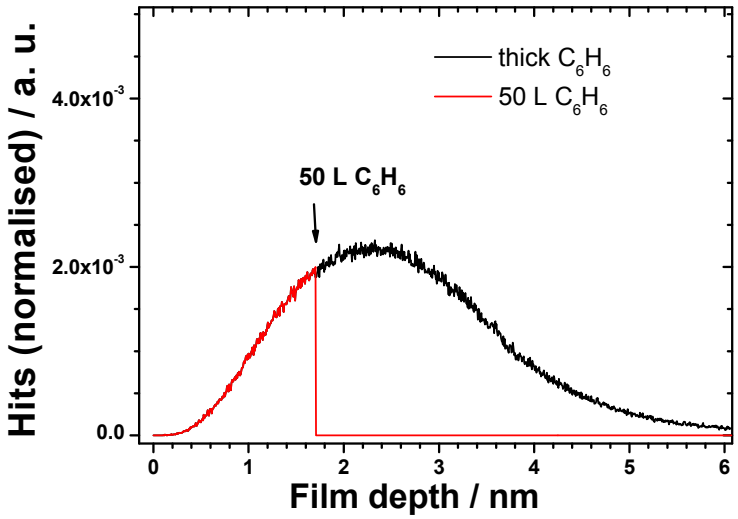

Figure 2 *Normalised distribution of the electrons as a function of the penetration depth during the irradiation of 200 L (7 nm) of C_6H_6 film. This curve (in black) was obtained for 250 eV electrons. The estimated average thickness of 50 L of C_6H_6 is highlighted in red. For all the exposures $<$ 50 L the incident beam is transmitted, almost unchanged, to the ASW underlayer.*

(1.7 nm) of C_6H_6. Therefore, for all the exposures lower than 50 L, most of the electrons will pass through the entire overlayer of C_6H_6 reaching the ASW substrate, while they are stopped inside the C_6H_6 bulk for a 200 L dose. It can be concluded that for the experiments reported in *section 3.2* of the article, where 5 L of C_6H_6 are deposited on top of the H_2O ice, any change in the flux of the incident beam reaching the H_2O layer due to the overlayer is negligible. This justifies the choice

of focusing on pure c-ASW ices for additional simulations.

The thinnest film employed in the experiments is a binary layered ice with 5 L of C_6H_6 and 70 L (7.7 nm) of c-ASW irradiated with 250 eV electrons. The results displayed in **Figure 3** show that the maximum of the distribution peaks around 3 nm and that almost all the electrons ($\sim$ 85%) are stopped within the top 5 nm for a pure c-ASW film. An almost vanishing tail persists until 10 nm

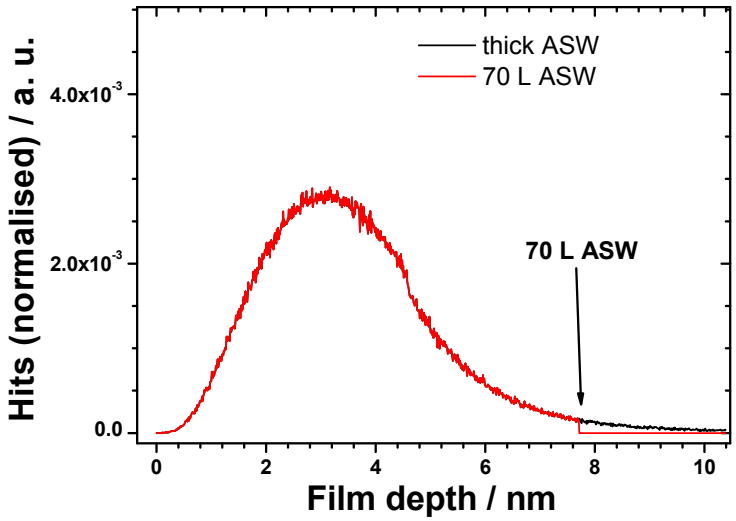

Figure 3 *Normalised distribution of the electrons as a function of the penetration depth during the irradiation of 100 L (11 nm) of c-ASW. This curve (in black) was obtained for 250 eV electrons. The estimated average thickness of 70 L of H_2O is highlighted in red. For all the exposures $>$ 70 L the incident beam is completely stopped by the c-ASW ice, while for a 70 L dose only the 2% of the primary electrons can pass through.*

where the curve decays to zero, but only 2% of the electrons is transmitted through the ASW ice for a 70 L dose. In all the other cases, the systems investigated have an overall larger thickness than the calculated electron maximum penetration depth.

It can be argued that the results reported in *section 3.1* were obtained following the irradiation of ices with 300 eV electrons and, hence the penetration depth can be larger than for 250 eV electrons. **Figure 4** displays the distribution of the primary 100 - 350 eV electrons as a function of the c-ASW thickness. The maximum depth increases with electron energy, and it is noticeable that for 300 eV and 350 eV the curves decay to zero at higher lengths ($\sim$ 14 nm). However, this depth is still smaller than the average thickness estimated for the 150 L (16.5 nm) of ASW used.

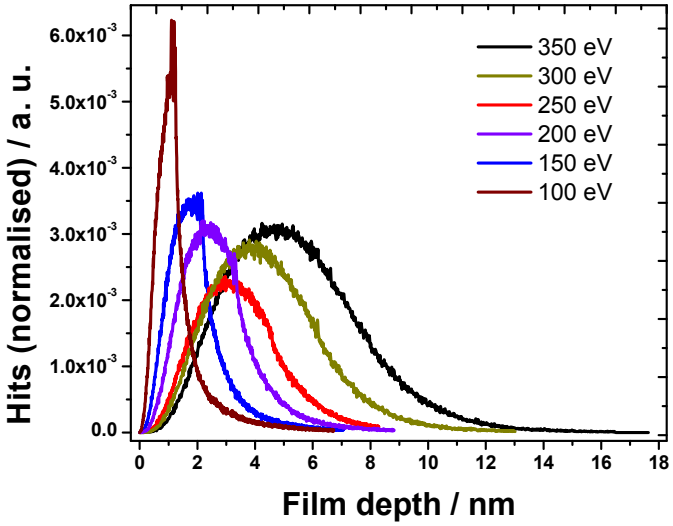

Figure 4 *Normalised distributions of the electrons as a function of the penetration depth during the irradiation of 200 L (22 nm) of c-ASW. These curves were obtained for different electron energies in the 100 eV - 350 eV range. For the 250 eV (in red) and 300 eV (in dark yellow) distributions all the electrons are stopped within the top 5 to 10 nm.*

3 SRIM Calculations

The reported irradiation experiments can be related to the secondary electron track that forms within the icy mantles that coat interstellar dust grains as a result of impinging cosmic rays (mainly protons). Therefore, in order to aid the discussion of the data and to make considerations in an astrophysical context, the SRIM code[9,10] allowed us to quantify the energy deposited by a single H^+ ion as a function of the initial ion energy (10 keV - 100 MeV). The H_2O solid model that was used is consistent with the CASINO calculations assuming the same molecular density. The output was then used to estimate how many secondary electrons are generated in a pure ASW film during H^+ ion bombardment under typical ISM conditions.

For an incident H^+ flux (10 keV - 100 MeV) all the energy is deposited through scattering with the electron density within the target molecular solid, while the energy lost by the primary ions because of the nuclear scattering is several orders of magnitude lower, as **Figure 5** clearly displays. The energy deposited in the film associated with all inelastic electronic events in 1 μm is 20 keV μm^{-1}. This, divided by the amount of energy transferred per ionisation event (22 eV[11,12]), and taking into account a penetration depth of 5 nm, gives the secondary electron yield of 4.5 electrons per incident proton. This yields a secondary electron flux (F_{e^-}) in c-ASW of 4.5 electrons cm^{-2} s^{-1} for 1 cm^{-2} s^{-1} 1 MeV H^+ incident ions. The value can be used in **Equation 6** in order to estimate the EPD rate constant.

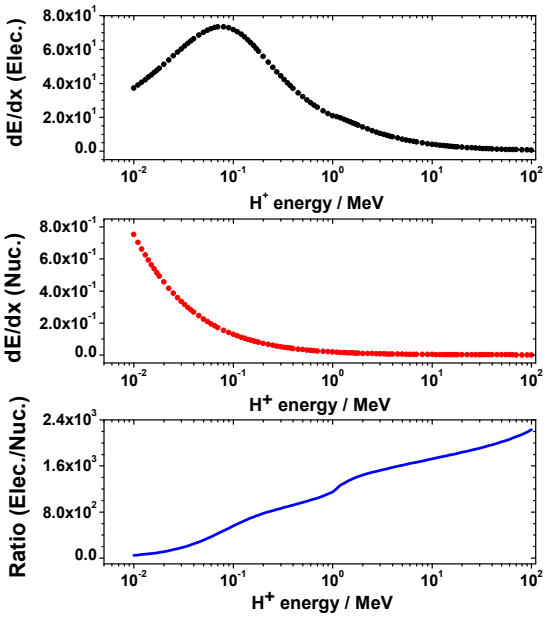

Figure 5 *The upper and central plot show the calculated energy deposited in c-ASW due to electron and nuclear scattering respectively per unit of distance (μm) travelled by the projectile particle. The latter is a positively charged ion (H^+) having energy between 10 keV and 100 MeV. The plot at the bottom displays the ratio between the energy deposited in the ice by the two inelastic scattering events showing the predominance of electron scattering in the energy range of interest for cosmic rays.*

References

[1] J. D. Thrower, M. P. Collings, F. J. M. Rutten and M. R. S. McCoustra, *J. Chem. Phys.*, 2009, **131**, 244711.

[2] J. D. Thrower, *PhD thesis*, Heriot-Watt University, 2009.

[3] *Theory of Condensed Matter Group Cambridge, CASINO V 2.48*, http://www.gel.usherbrooke.ca/casino/What.html, 2014.

[4] P. Hovington, D. Drouin and R. Gauvin, *Scanning*, 1997, **19**, 1–14.

[5] G. D. Waddill and L. L. Kesmodel, *Phys. Rev. B*, 1985, **31**, 4940–4946.

[6] C. J. Craven, P. D. Hatton, C. J. Howard and G. S. Pawley, *J. Chem. Phys.*, 1993, **98**, 8236–8243.

[7] R. L. Summers, *Empirical observations on the sensitivity of hot cathode ionization type vacuum gauges*, National Aeronautics and Space Administration, Washington, D. C., 1969.

[8] G. A. Kimmel, Z. Dohnálek, K. P. Stevenson, R. S. Smith and B. D. Kay, *J. Chem. Phys.*, 2001, **114**, 5295–5303.

[9] J. F. Zigler, *SRIM/TRIM*, http://www.srim.org, 2013.

[10] J. F. Ziegler, J. P. Biersack and M. D. Ziegler, *The Stopping and Range of Ions in Solids*, Pergamon Press, New York, 2008.

[11] W. F. Schmidt and E. Illenberger, *Nukleonika*, 2003, **48**, 75–82.

[12] M. Vinodkumar, K. N. Joshipura, C. G. Limbachiya, and B. K. Antony, *Nucl. Instrum. Methods Phys. Res. B*, 2003, **212**, 63–66.